



Tenth U.S. National Conference on Earthquake Engineering  
Frontiers of Earthquake Engineering  
July 21-25, 2014  
Anchorage, Alaska

# GROUND MOTION MODELING FOR RISK AND RELIABILITY ASSESSMENT OF SAN FRANCISCO INFRASTRUCTURE SYSTEMS

J. Wu<sup>1</sup> and J.W. Baker<sup>2</sup>

## ABSTRACT

Infrastructure network resilience to major hazards, such as earthquakes, is a critical attribute that impacts the magnitude and extent of direct and indirect losses as well as post-disaster recovery. However, network resilience estimation is a nontrivial issue due to the uncertainty of hazards and the complexity of the response of large networks to perturbation. This research details a methodology to evaluate the resilience of networks subjected to seismic hazards by combining the most recent hazard and risk estimation techniques. This paper focuses on the ground motion intensity simulation aspect of the research, which utilizes current rupture forecasts and ground motion prediction equations in conjunction with a ground motion spatial correlation model. Recent research reports that ground motion estimation using solely median values without consideration of spatially correlated residuals may be inadequate in characterizing seismic events within a region; thus, this research rigorously pursues accurate spatial correlation representation through the proposed ground motion model. This model is used to generate realistic ground motion intensity maps considering a wide range of earthquake scenarios to supplement existing maps in the San Francisco area to enhance the rigor and merit of subsequent network reliability analysis. This research lays the groundwork for future assessments of critical infrastructure networks, which aims to provide insight regarding efficient retrofit of networks to improve their resilience to seismic hazards and expedite post-disaster recovery.

---

<sup>1</sup>Ph. D. Student, Dept. of Civil and Env. Eng., Stanford University, Stanford, CA 94305, [jwu11@stanford.edu](mailto:jwu11@stanford.edu)

<sup>2</sup>Associate Professor, Dept. of Civil and Env. Eng., Stanford University, Stanford, CA 94305, [bakerjw@stanford.edu](mailto:bakerjw@stanford.edu)

# GROUND MOTION MODELING FOR RISK AND RELIABILITY ASSESSMENT OF SAN FRANCISCO INFRASTRUCTURE SYSTEMS

J. Wu<sup>1</sup> and J. W. Baker<sup>2</sup>

## ABSTRACT

Infrastructure network resilience to major hazards, such as earthquakes, is a critical attribute that impacts the magnitude and extent of direct and indirect losses as well as post-disaster recovery. However, network resilience estimation is a nontrivial issue due to the uncertainty of hazards and the complexity of the response of large networks to perturbation. This research details a methodology to evaluate the resilience of networks subjected to seismic hazards by combining the most recent hazard and risk estimation techniques. This paper focuses on the ground motion intensity simulation aspect of the research, which utilizes current rupture forecasts and ground motion prediction equations in conjunction with a ground motion spatial correlation model. Recent research reports that ground motion estimation using solely median values without consideration of spatially correlated residuals may be inadequate in characterizing seismic events within a region; thus, this research rigorously pursues accurate spatial correlation representation through the proposed ground motion model. This model is used to generate realistic ground motion intensity maps considering a wide range of earthquake scenarios to supplement existing maps in the San Francisco area to enhance the rigor and merit of subsequent network reliability analysis. This research lays the groundwork for future assessments of critical infrastructure networks, which aims to provide insight regarding efficient retrofit of networks to improve their resilience to seismic hazards and expedite post-disaster recovery.

## Introduction

Infrastructure network resilience and reliability are crucial in mitigating both physical and economic damage and expediting recovery from major disasters, such as hurricanes, terrorist attacks, and earthquakes. Not only would a resilient network minimize damage and hasten the restoration of its components, but also facilitate the recovery of other infrastructure networks. Dueñas-Osorio and Kwasinski [1] report significant operational interdependencies between networks from analyzing post earthquake restoration curves. Network resilience and swift recovery helps mitigate indirect losses in the commercial sector due to business interruption. Resilient water delivery and electrical power networks help minimize the financial losses that would accrue daily due to facility shutdown. Business activities such as the production and transport of goods may resume sooner with a reliable transportation network. Furthermore, post

---

<sup>1</sup>Ph. D. Student, Dept. of Civil and Env. Eng., Stanford University, Stanford, CA 94305, jwu11@stanford.edu

<sup>2</sup>Associate Professor, Dept. of Civil and Env. Eng., Stanford University, Stanford, CA 94305, bakerjw@stanford.edu

disaster network operability may be crucial in maintaining safety and health of the community after the primary event. Engineers must be able to access structures to evaluate their safety and integrity, while essential healthcare facilities (e.g. hospitals) rely on the functionality of power, water, and wastewater systems to maintain their services [2-3]. In the case of earthquakes, while strong ground motion does induce heavy damage in structures, a significant source of damage may be attributed to fires following the earthquake. It is reported that the 1906  $M_w$  7.8 San Francisco earthquake destroyed 28,000 buildings in San Francisco, 80% of which were attributed to the fires induced by the earthquake. A seismically resilient water delivery system would be able to provide the resources to help combat these fires, whereas resilient telecommunication and transportation networks would better provide personnel with the required information and mobility to accommodate the sites requiring assistance.

Thus, this research seeks to determine the means of improving network resiliency through the analysis of the seismic performance of infrastructure networks, using San Francisco as an example, by combining the most recent hazard and risk estimation techniques. This network analysis follows the methodology described in Miller and Baker [4], which may be generalized in the following steps: 1) Generate earthquake scenarios; 2) Generate ground motion maps for each scenario using ground motion prediction equations (GMPEs) and associated intra- and inter-event residuals; 3) Simulate damage states of structures using the ground motion maps and appropriate fragility estimates; 4) Compute network performance using the simulated damage on its components. This paper discusses the ground motion map generation aspect of the research.

Past research analyzes network resilience by subjecting networks to past earthquake events/scenario earthquakes [5-8], varying ground motion intensity values [9-11], or a combination of the two [12]. In this research, the authors simulate spatially correlated realizations of ground motion intensities based on an extensive list of potential earthquakes to evaluate the performance of San Francisco networks. This list of earthquake scenarios comes from the UCERF2 source model [13], and includes many rupture scenarios of moment magnitudes from 5.35 to 8.25, and on all faults in the region, including the North San Andreas Fault, Hayward Fault, and Calaveras Fault. Additionally, using only median ground motion values or evaluating ground motion intensities at each site individually is insufficient as described in previous research [14-17], and Park et al. [18] reports that ignoring or underestimating spatial correlation overestimates frequent losses and underestimates rare ones. Thus, spatial correlation effects are rigorously pursued and implemented into the simulation process in this research to yield a more accurate hazard assessment.

The remainder of this paper is structured as follows. First, procedures for constructing ground motion intensity maps and applying spatial correlation are outlined. The paper continues with a discussion and comparison of the ground motion maps currently available for San Francisco networks with the ground motion simulations pursued in this paper. Finally, this paper concludes with a brief discussion on the limitations of the current ground motion model and the application of the generated ground motion intensity maps to future phases of this research.

## **Ground Motion Simulation**

This section discusses the methods of simulating spatially correlated ground motion maps pursued in this research. Ground motion simulation begins with the assembly of a portfolio of sites located in the vicinity of the network of interest at which ground motion intensities are evaluated. The ground motion intensities are simulated at each site using the model described in Eq. 1 that predicts intensities at a site  $i$  due to an earthquake  $j$  as formulated in previous research [19-21]:

$$\ln Y_{ij} = \ln \bar{Y}_{ij} + \sigma_{ij}\varepsilon_{ij} + \tau_j\eta_j \quad (1)$$

where  $Y_{ij}$  is the estimated ground motion value (such as peak ground acceleration, PGA),  $\bar{Y}_{ij}$  is the median ground motion value,  $\sigma_{ij}\varepsilon_{ij}$  describes the within-event residual, and  $\tau_j\eta_j$  describes the between-event residual [22]. Inside the residual terms,  $\tau_j$  is the between-event standard deviation, while  $\sigma_{ij}$  is the within-event standard deviation. The  $\eta_j$  and  $\varepsilon_{ij}$  terms are random variables sampled during ground motion simulation.

Median values of ground motion intensities at each site are derived from formulated GMPEs which generally consider earthquake magnitude, distance to rupture, fault parameters, and geological conditions. Random realizations of scatter around the median values are then applied using within-event and between-event log standard deviation values (also from GMPEs) and associated random variables  $\eta_j$  and  $\varepsilon_{ij}$ , yielding a possible ground motion intensity map. Median and log standard deviation values of ground motion derived from various GMPEs for various earthquake scenarios are obtained using applications developed by OpenSHA [23], an open-source Java-based platform for conducting seismic hazard analysis. The  $\eta_j$  term is a random variable that follows a standard normal distribution ( $\mu = 0$  and  $\sigma = 1$ ), while the  $\varepsilon_{ij}$  term is regarded as a 2-dimensional random field that exhibits spatial correlation following a model semivariogram—a measure of the average dissimilarity in data values as a function of separation distance between sites [24].

Jayaram and Baker [19] analyze isotropic semivariograms of ground motion from past earthquakes and proposed the semivariogram presented in Eq. 2 for predicting correlations in future ground motions with a given separation distance.

$$\gamma(h_{xy}) = 1 - \exp(-3h_{xy}/b) \quad (2)$$

where  $h_{xy}$  is the distance between sites  $x$  and  $y$ , and  $b$  is a factor that depends on the ground motion intensity measure calculated as well as geological homogeneity, assessed by the clustering in  $V_{s30}$  values—average shear wave velocities in the top 30 meters of soil. This paper simulates intensity maps describing the distribution of PGA within a region that exhibits clustering in  $V_{s30}$ , and thus  $b$  is calculated using Eq. 3:

$$b = 40.7 - 15.0T \quad (3)$$

where  $T$  is the spectral period (in seconds) of the ground motion intensity measure. For PGA,  $T$  is equal to 0, and thus  $b$  is calculated to be 40.7. To construct the  $\varepsilon_{ij}$  term that follows the model semivariogram from Eq. 2, this research pursues the following two approaches: the *covariance formulation* and the *spectral formulation*.

## Spatially Correlated Simulations using the Covariance Formulation

Jayaram and Baker [19] constructs the  $\varepsilon_{ij}$  term that reflects the model semivariogram in Eq. 2 by sampling from a multivariate normal distribution with a mean vector  $\{0\}$  and covariance matrix defined by Eq. 4:

$$\Sigma_{xy} = 1 - \gamma(h_{xy}) = \exp(-3h_{xy}/b) \quad (4)$$

where  $\Sigma_{xy}$  is the covariance between sites  $x$  and  $y$ , stored as the  $(x^{\text{th}}, y^{\text{th}})$  element of the covariance matrix  $\Sigma$ , and  $h_{xy}$  and  $b$  are the same as those in Eq. 2. This method is denoted as the *covariance formulation*, as spatial correlation is implemented through the covariance matrix of the multivariate normal distribution. Fig. 1 below depicts a spatially correlated ground motion map simulated using this formulation. Fig. 1 (a) depicts the median PGA obtained from a moment magnitude 7.9 earthquake due to a full rupture of the North San Andreas Fault using the GMPE formulated by Boore and Atkinson [25] ( $\bar{Y}_{ij}$  from Eq. 1). Fig. 1 (b) depicts the contribution of a realization of the between-event and within-event residuals ( $\sigma_{ij}\varepsilon_{ij}$  and  $\tau_j\eta_j$  from Eq. 1) to the ground motion realization. Fig. 1 (c) depicts a realization of PGA after the application of the between-event and within-event residuals in Fig 1. (b) to the median values in Fig.1 (a) ( $Y_{ij}$  from Eq. 1).

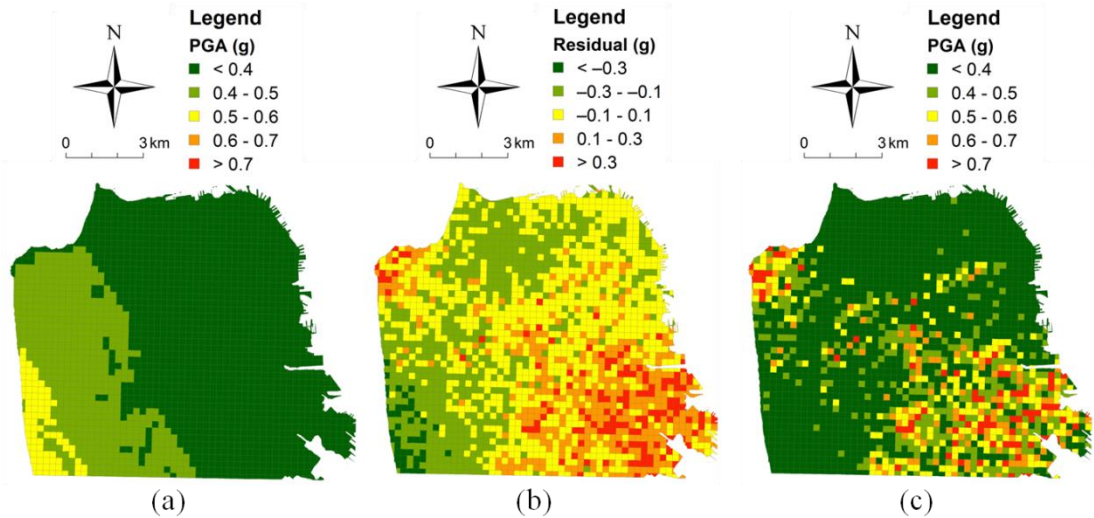


Figure 1. Peak ground acceleration values using the GMPE from Boore and Atkinson (2008) for an  $M_w$  7.9 earthquake induced by a full rupture of the North San Andreas Fault. (a) depicts the median PGA values while (b) depicts a realization of the between-event and within-event residuals and (c) depicts a realization of PGA after implementing the between-event and within-event residuals to the median values.

While this method produces the desired correlation in the ground motion realizations, one significant issue is the amount of resources required for the calculation of the correlated  $\varepsilon_{ij}$  terms—as the number of sites increases, the random sampling of  $\varepsilon_{ij}$  becomes a nontrivial procedure. The governing source of computational expense is the calculation of the covariance

matrix of size  $n \times n$ , where  $n$  is the number of sites. Thus, the computational expense (in terms of both memory and time) of larger ground motion maps will increase in  $O(n^2)$ . This research explores alternate methods such to mitigate computational expense while maintaining reasonable accuracy.

### Spatially Correlated Simulations using the Spectral Formulation

Rather than constructing the full  $n \times n$  covariance matrix, the *spectral formulation* utilizes Fourier transform methods to approximate the spatial correlation of  $\varepsilon_{ij}$  realizations. One requirement for the application of the spectral formulation is that the sites must be arranged in a regularly spaced square grid. The general procedure is described in the following steps:

- 1) Calculate a matrix containing the covariance values between a site at one corner of the grid with every other site, yielding a square matrix with  $n$  elements, where  $n$  is the number of sites.
- 2) Perform a two-dimensional fast Fourier transform on the covariance values.
- 3) Generate independent random Fourier coefficients for each spectral period by sampling from a normal distribution with mean 0 and variance calculated as a function of the Fourier transformed covariance values from step 2.
- 4) Obtain the two-dimensional random field by from an inverse fast Fourier transform.

More details on this procedure may be found in Fenton [26].

Most of the computational effort is associated with the Fourier transform and the simulation of the Fourier coefficients, which appears to be approximately  $O(n)$ , a vast improvement over the computational effort of the covariance formulation. Fig. 2 below compares the computation time and memory usage between the two methods:

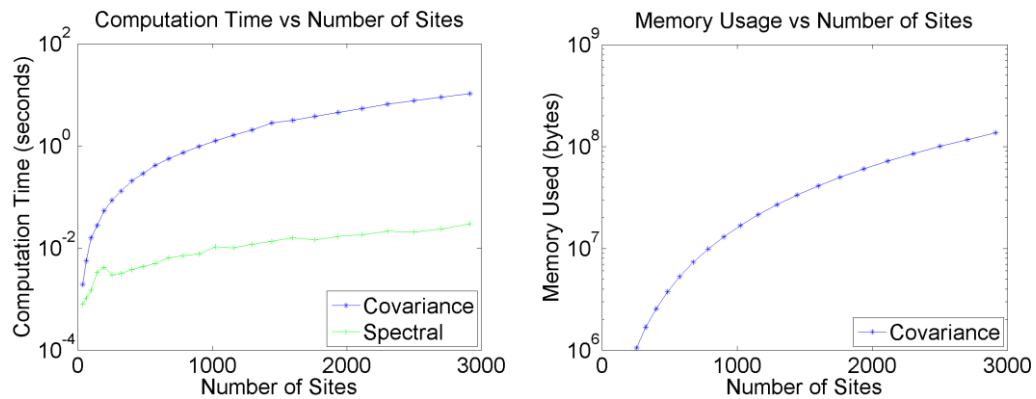


Figure 2. (a) Computation time and (b) memory usage for the simulation of a 2-D random field using the spectral and covariance formulations. Note that (b) does not depict the spectral method—this is due to the memory usage of the spectral method being too small to be captured within MATLAB for the given number of sites.

However, the spectral formulation introduces a slight deviation from the desired spatial correlation of the random field, as may be seen in Fig. 3 (a) and (b), which depict realizations of

random fields using the covariance and spectral formulations. This figure allows for a quick visual comparison of the random fields generated by the proposed methods. A noticeable difference between Fig. 3 (a) and (b) may be discerned—the random field produced by the spectral method appears more “burry” as compared to that produced by the covariance method, signifying inconsistent spatial correlation between the two methods, especially at small distances. These observations are supported by results depicted in Fig. 4, which compare the model semivariogram (given in Eq. 2) with the experimental semivariograms calculated from the generated random fields using Eq. 5 given below [19]:

$$\hat{\gamma}(h) = \frac{1}{2N(h)} \sum_{\alpha=1}^{N(h)} [z_{u_\alpha} - z_{u_\alpha+h}]^2 \quad (5)$$

where  $\hat{\gamma}(h)$  is the experimental semivariogram,  $z_u$  is the value at location  $u$ ,  $N(h)$  is the number of pairs of sites separated by a distance  $h$ , and  $[z_{u_\alpha}, z_{u_\alpha+h}]$  is the  $\alpha^{\text{th}}$  such pair.

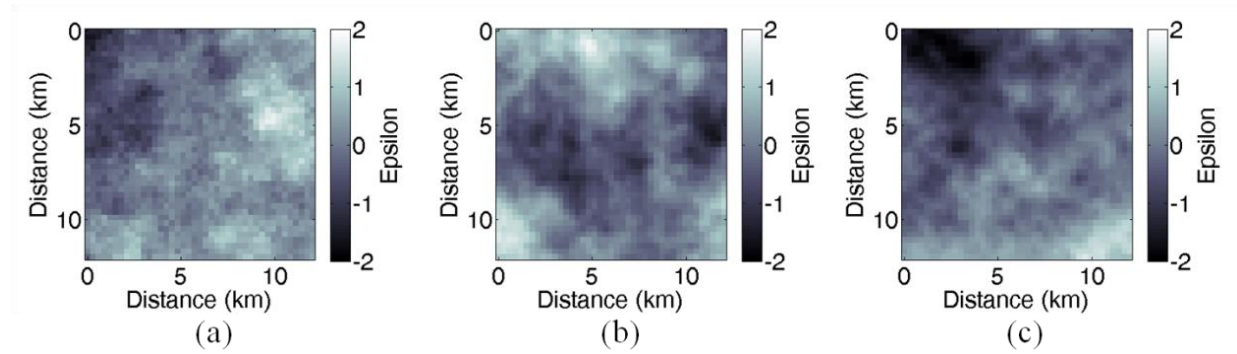


Figure 3. Spatially correlated random fields of sites arranged in a 41 x 41 grid with 300 meter spacing between sites generated using (a) the covariance formulation, (b) the spectral formulation, and (c) the scaled spectral formulation.

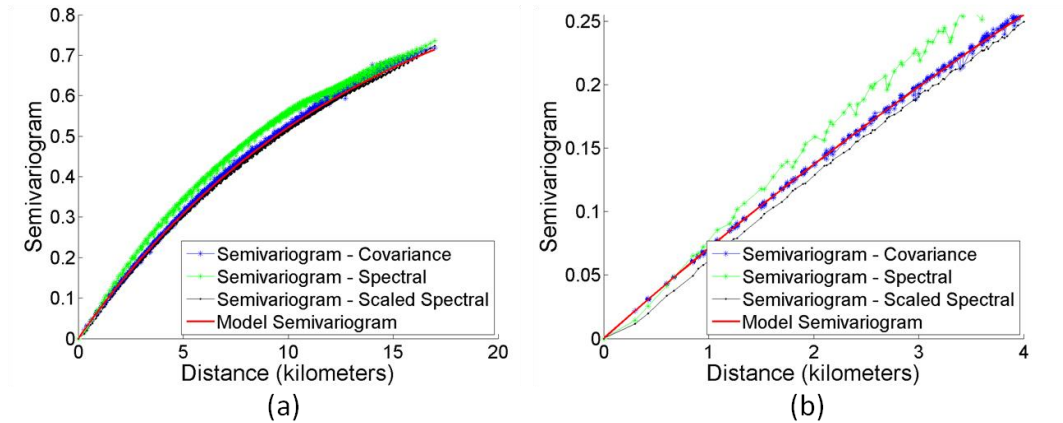


Figure 4. Model semivariogram compared to the average experimental semivariograms of 1000 random fields generated using covariance formulation, unscaled spectral formulation, and scaled spectral formulation for sites arranged in a 41 x 41 grid with 300 meter spacing between sites. (a) depicts the semivariogram for the entire domain of separation distances, while (b) depicts the semivariogram at small distances.

As can be seen in Fig. 4, the experimental semivariogram using the covariance formulation matches the model semivariogram fairly well, whereas the spectral formulation appears to underestimate the semivariogram (or overestimate the spatial correlation) at very small distances and overestimate the semivariogram at larger distances. One method of addressing this issue suggested in [26] is to increase the size of the random field and discard the excess values, as the semivariogram from the spectral formulation converges towards the model semivariogram with increased field size. The resulting random field is depicted by Fig. 3 (c), in which the size of the field is increased by a factor of 3, and the resulting experimental semivariogram is depicted in Fig. 4. Again, upon visual inspection of the resulting random fields, the spatial correlation still appears inconsistent between the covariance and scaled spectral methods. Observing Fig. 4, increasing the size of the spectral formulation yields an experimental semivariogram that better matches the model semivariogram as compared to the semivariogram from the unscaled spectral formulation; however, this solution still appears imperfect as the experimental semivariograms still slightly deviate from the model semivariogram. Future work will continue to refine the simulation of correlated random fields to address this issue.

### CAPPS Ground Motion Maps

The correlated ground motion simulations pursued in this paper serve to supplement the existing ground motion maps for San Francisco such as those derived from the earthquake scenarios described in the Applied Technology Council’s (ATC) technical documentation for the Community Action Plan for Seismic Safety (CAPPS) Project discussing earthquake impacts on San Francisco [27]. An example ground motion map is depicted in Fig. 5, describing the median PGA induced by a rupture on the North San Andreas Fault.

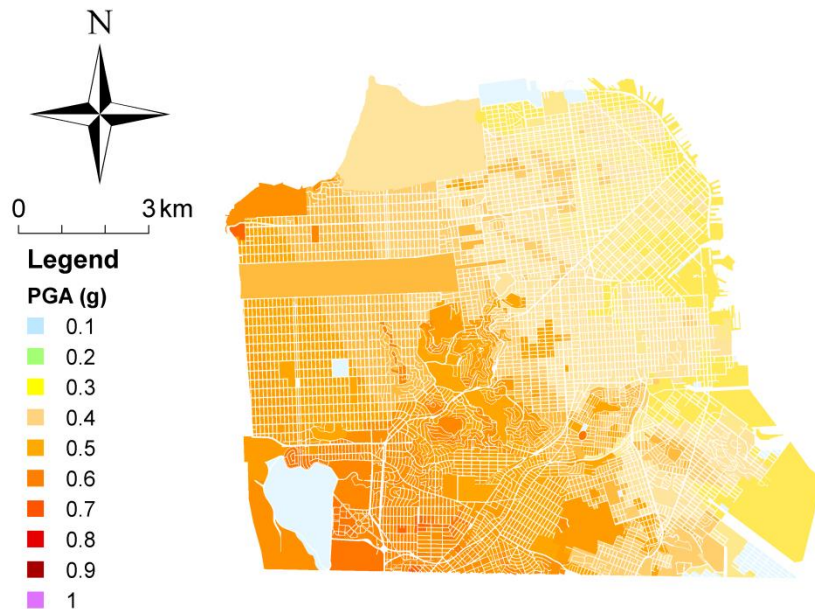


Figure 5. Median PGA in the San Francisco area due to an  $M_w$  7.9 earthquake on the North San Andreas Fault.

The CAPPS report considers four earthquake scenarios—three ruptures on the North San Andreas Fault and one on the Hayward Fault, while more exhaustive sampling of sources in the area (e.g., using OpenSHA) can produce more than 2000 earthquake scenarios for the San Francisco area, from which a subset could be selected using methods described in Miller and Baker [4] or Han and Davidson [28]. Thus this research supplements the existing ground motion maps with a broader set of earthquake scenarios for higher scrutiny of network design and performance. Additionally, existing ground motion maps typically neglect spatial correlation of ground motion; these maps, though simple to compute and utilize, may be unrealistic as previously mentioned. Thus, through the rigorous simulation of ground motion values with correlated residuals, this research contributes realistic ground motion maps for a more meaningful analysis of the San Francisco infrastructure networks.

## Conclusion

This paper showcases the combination of the most recent tools and methods to perform ground motion simulation: calculation of the median and dispersion values of ground motion intensities using various GMPEs and earthquake events compiled by OpenSHA; introduction of spatial correlation into the ground motion intensity values by means of a correlated two-dimensional random field; and the formulation of the correlated two-dimensional random field by either sampling from a correlated multivariate normal distribution (covariance formulation) or utilizing Fourier transform techniques to randomize the relative contribution of spectral components to the random field (spectral formulation). These efforts contribute to subsequent network analysis through the consideration of a wide range of earthquake scenarios and the implementation of spatial correlation to yield more realistic ground motion maps.

Limitations of this methodology include the computational expense of simulating the correlated residuals for a large portfolio of sites, as seen in Fig. 2. The computation time for simulating these ground motion maps may not be a critical factor as compared to the computation time for network analysis for which these ground motion maps are generated; however, memory usage is a significant issue, as the covariance formulation requires several megabytes of memory for a modest number of sites, and ground motion maps for a much larger number of sites may be required and for which the covariance formulation may not accommodate. This research explores alternate methods of simulating the correlated residuals by utilizing Fourier transform techniques. However, this method sacrifices accuracy in spatial variability for reduced computational expense. This deviation may be mitigated by increasing the size of the random field and discarding the excess data, as the experimental semivariogram for the spectral formulation converges towards that of the covariance formulation with larger field size. Even after increasing the size of the random field by a reasonable amount, the runtime of the spectral formulation remains substantially less than that of the covariance formulation, thus maintaining computational efficiency while mitigating the error in spatial correlation. However, as seen in Figs. 3 and 4, this process is still imperfect, as it introduces undesirable deviations in the spatial correlation between sites. Additional means of addressing this issue include implementing weighting functions to the Fourier coefficients as described in Bruining et al. [29] or pursuing Sequential Simulation techniques as described in Jayaram [30].

The ground motion simulation methodology described in this paper is but the initial step for analyzing and estimating infrastructure network performance and resilience to seismic events. Simulated ground motion intensity maps are utilized in the estimation of network component damage and subsequent network level performance metrics. This research intends to showcase the numerous and complex interactions between the various risk and hazard models as well as demonstrate the application of the most recent methodologies for all phases of the network analysis to lay the groundwork for future network analyses. Network resilience analysis provides insight on the highly complex response of infrastructure networks incalculable through direct means, and the results of such analyses provide insights regarding efficient allocation of resources and thoughtful retrofit of existing infrastructure to improve performance and post-disaster recovery.

### Acknowledgments

This work was supported in part by the National Science Foundation under NSF grant number CMMI 0952402. Any opinions, findings and conclusions or recommendations expressed in this material are those of the authors and do not necessarily reflect the views of the National Science Foundation. The authors thank the San Francisco Public Utilities Commission for their data and technical discussions. The authors also acknowledge technical support provided by Dr. Mohammad Javanbarg of AIG, Dr. Thomas O'Rourke of Cornell University, and Mahalia Miller and Christophe Loth of Stanford University.

### References

1. Dueñas-Osorio L, Kwasinski A. Quantification of lifeline system interdependencies after the 27 February 2010 Mw 8.8 offshore Maule, Chile, earthquake. *Earthquake Spectra* 2012; **28** (S1): S581-S603.
2. Jacque C et al. Resilience of the Canterbury Health Care System to the 2011 Christchurch (Mw=6.2) Earthquake, NZ. *Earthquake Spectra*. In Press.
3. Mitrani-Reiser J et al. Response of the Regional Health Care system to the 22nd February 2011, Christchurch Earthquake, NZ. *Proceedings of the 15<sup>th</sup> World Conference on Earthquake Engineering*, Lisbon, Portugal, 2012.
4. Miller M, Baker JW. A framework for selecting a suite of ground-motion intensity maps consistent with both ground-motion intensity and network performance hazards for infrastructure networks. *11th International Conference on Structural Safety & Reliability*, New York, NY, 2013.
5. Kim Y, Kang, W-H, Song J. Assessment of seismic risk and importance measures of interdependent networks using a non simulation-based method. *Journal of Earthquake Engineering* 2012; **16** (6): 777-794.
6. Wu J, Dueñas-Osorio L. Calibration and validation of a seismic damage propagation model for interdependent infrastructure systems. *Earthquake Spectra* 2013; **29** (3): 1021-1041.
7. Adachi T, Ellingwood BR. Serviceability of earthquake-damaged water systems: Effects of electrical power availability and power backup system on system vulnerability. *Reliability Engineering and System Safety* 2008; **93**: 78-88.
8. Bonneau A, O'Rourke TD. *Water supply performance during earthquakes and extreme events, Technical Report MCEER-09-0003*. MCEER: New York, 2009.
9. Selva J, Kakderi K, Alexoudi M, Pitilakis K. Seismic performance of a system of interdependent lifeline and infrastructure components. *Proceedings of the 8<sup>th</sup> International Conference on Urban Earthquake Engineering*, Tokyo Institute of Technology, Tokyo, Japan, 2011.

10. Fragiadakis M, Christodoulou SE. Seismic reliability assessment of urban water networks. *Earthquake Engineering and Structural Dynamics* 2013.
11. Hernandez-Fajardo I, Dueñas-Osorio L. Sequential propagation of seismic fragility across interdependent lifeline systems. *Earthquake Spectra* 2011; **27** (1): 23-43.
12. Song J, Ok S-Y. Multi-scale system reliability analysis of lifeline networks under earthquake hazards. *Earthquake Engineering and Structural Dynamics* 2010; **39**: 259-279.
13. Field EH et al. Uniform California Earthquake Rupture Forecast. *Bulletin of the Seismological Society of America* 2009; **99** (4): 2053-2107.
14. Bommer JJ, Crowley H. The influence of ground-motion variability in earthquake loss modeling. *Bulletin of earthquake Engineering* 2006; **4**: 231-248.
15. Goda K, Hong HP. Spatial correlation of peak ground motions and response spectra. *Bulletin of the Seismological Society of America* 2008; **98** (1): 354-365.
16. Bazzurro P, Luco N. Effects of different sources of uncertainty and correlation on earthquake-generated losses. *Presented at IFED: International Forum on Earthquake Decision Making*, Stoos, Switzerland, 2004.
17. Baker JW, Miller M. Effects of earthquake source geometry and site conditions on spatial correlation of earthquake ground motion hazard. *Keynote lecture at 4th IASPEI/IAEE International Symposium on Effects of Surface Geology on Seismic Motion*, Santa Barbara, California, 2011
18. Park J, Bazzurro P, Baker JW. Modeling spatial correlation of ground motion intensity measures for regional seismic hazard and portfolio loss estimation. *Tenth International Conference on Application of Statistic and Probability in Civil Engineering*, ICASP10, Tokyo, Japan, 2007.
19. Jayaram N, Baker JW. Correlation model for spatially distributed ground-motion intensities. *Earthquake Engineering and Structural Dynamics* 2009; **38**: 1687-1709.
20. Loth C, Baker JW. A spatial cross-correlation model of ground motion spectral accelerations at multiple periods. *Earthquake Engineering and Structural Dynamics* 2013; **42** (3): 397-417.
21. Abrahamson NA, Youngs RR. A stable algorithm for regression analyses using the random effects model. *Bulletin of the Seismological Society of America* 1992; **82** (1): 505-510.
22. Al Atik L, Abrahamson N, Bommer JJ, Scherbaum F, Cotton F, Kuehn N. The variability of ground-motion prediction models and its components. *Seismological Research Letters* 2010; **81**(5): 794-801.
23. Field EH, Jordan TH, Cornell CA. OpenSHA: A developing community-modeling environment for seismic hazard analysis. *Seismological Research Letters* 2003; **74** (4): 406-419.
24. Goovaerts P. *Geostatistics for Natural Resources Evaluation*. Oxford University Press: Oxford, New York, 1997.
25. Boore DM, Atkinson GM. Ground-motion prediction equations for the average horizontal component of PGA, PGV, and 5%-Damped PSA at spectral periods between 0.01s and 10.0s. *Earthquake Spectra* 2008; **24** (1): 99-138.
26. Fenton GA. *Simulation and Analysis of Random Fields*. Ph. D. Dissertation, Princeton University: New Jersey, 1990.
27. Applied Technology Council 52-1A. *Here Today, Here Tomorrow: The Road to Earthquake Resilience in San Francisco*. ATC: San Francisco, California, 2010.
28. Han Y, Davidson RA. Probabilistic seismic hazard analysis for spatially distributed infrastructure. *Earthquake Engineering and Structural Dynamics* 2012; **41**: 2141-2158.
29. Bruining B, Van Batenburg D, Lake LW, Yang AP. Flexible spectral methods for the generation of random fields with power-law semivariograms. *Mathematical Geology* 1997; **26** (6): 823-848.
30. Jayaram N, *Probabilistic Seismic Lifeline Risk Assessment Using Efficient Sampling and Data Reduction Techniques*. Ph. D. Dissertation, Stanford University: California, 2010.